Robotica (2015) volume 33, pp. 1424–1445. © Cambridge University Press 2014
doi:10.1017/S0263574714000848

Joints flexibility effect on the dynamic performance of robots

Mohamed H. Zaher* and Said M. Megahed

Mechanical Design and Production Engineering Department, Cairo University, Giza 12613, Egypt

(Accepted March 7, 2014. First published online: April 8, 2014)

SUMMARY
This paper studies the effect of joint flexibility on the dynamic performance of a serial spatial robot arm of rigid links. Three models are developed in this paper. The first and the third models are developed using the multibody dynamics approach, while the second using the classical robotics approach. A numerical algorithm and an experimental test-rig are developed to test the final model. The links' inertial parameters are estimated numerically. Empirical formulae with assumption models are used to estimate the flexibility coefficients. The simulation results show that the joint damping is a major source of inaccuracies, causing trajectory error without a proper feedback controller.

KEYWORDS: Flexible joint; Robot; Multibody; Modeling; Kinematically constrained dynamic system simulation; Denavit–Hartenberg.

1. Introduction

As modern applications of robotics require a higher level of accuracy, the proper modeling of joints' flexibility is of utmost importance. Spong[1] presented the basis for modeling joints flexibility; however, the model neglects the effect of the dynamics of the preceding links and rotors, which limits it to slow motion robotic aplications. Comparative to their work, Ciuca *et al.*[2] represented the joint flexibility as a linear torsional spring assuming that the kinetic energy of each rotor is only due to its rotation. This assumption does not take the effect of the preceding links and rotors' kinematics into consideration. Correspondingly, both models of Spong[1] and Ciuca *et al.*[2] neglect the gyroscopic effects adopted by many researches to deal with different control problems. Among the research work that took the gyroscopic effect is that of Potkonjak[3] and Jankowski and Van Brussel.[4] Potkonjak[3] presented the transmission system while including the gyroscopic effect of the flexible joint while Jankowski and Van Brussel[4] presented the gyroscopic effects resulting from the rotor rotation while linearizing and decoupling the nonlinear-coupled dynamic system. Subudhi and Morris[5] improved on the complexity of the robotic models and considered the effects of flexibility in both links and joints. In addition, they considered the payload and structural damping of the links using Euler–Lagrange formulation and assumed modes discretization technique. However, the backlash in the reduction gear and coulomb friction are neglected. Flores *et al.*[6] focused on the joint model accuracy and studied the dynamics of a mechanical system with revolute joint clearance considering the dry contact, friction, and hydrodynamic lubrication effects using journal bearings as the revolute joint. Heidari and Nikoobin[7] combined the direction of work of Ciuca *et al.*[2] and Subudhi and Morris.[5] They determined the maximum allowable dynamic load for flexible link–flexible joint manipulators along a predefined trajectory while imposing the amplitude of residual vibration, actuator torque capacity, and end-effector precision. They used the finite element method to model the flexible links, but used a torsional spring to model joint flexibility. Le Tien *et al.*[8] introduced a friction observer to increase the positioning accuracy and the performance of torque control. The observer output corresponds to the low-pass filtered friction torque which is used for friction compensation in conjunction with a MIMO (multiple input, multiple output) controller designed for flexible joints. The friction compensation has several advantages as avoiding saturation and/or overflow of the integrator in case of external

* Corresponding author. E-mail: mhzaher@asme.org

disturbance torques. In addition, it can be used by impedance control in contact with the environment. Melhem and Loria[9] proposed a model for flexible joint robots, which is linear in the velocities instead of quadratic in the generalized velocities, as an attempt to overcome the technical difficulties. However, this proposed model is uncontrollable and unobservable in the Cartesian positions, orientations, and velocities.

On the control algorithm side, Ott *et al.*[10] proposed impedance controllers for flexible joint robots. They considered the stiffness and damping without inertia shaping. They designed the controllers separately for the stiffness and damping terms and the gravity compensation term. Their controller is designed to include some extensions to be usable with viscoelastic joints. Ider and Korkmaz[11] showed that the acceleration level inverse dynamics equations of parallel robots with flexible joint drives are singular as a result of the control torques delayed effect on the end-effector accelerations due to the joint flexibility. They proposed a control law with position and velocity feedback to decouple and linearize the system equations and achieve asymptotic stability. However, they did not measure the joint accelerations and jerks and relied on their calculations from the dynamic equations. Dahai and Xiaoping[12] tracked and identified the joint physical parameters of their robot real time for controlling vibration of their robot. They used an on-line identification method of frequencies and mode shapes of time-varying structure system which is based on modern harmonic identification. They computed the dynamic stiffness and dynamic damping by calculating the displacement and force balance. Yang *et al.*[13] presented a self-adapting robot arm control to attain natural adaptive motions as a controller employing neural oscillators. They tested their controller by showing the performance of a flexible joint robot arm coupled with neural oscillators through various tasks. Talole *et al.*[14] used feedback linearization to implement a state observer to track the trajectory of a single link flexible joint robot. One drawback of this method is the loss of performance and accuracy in the presence of modeling uncertainties. Akyuz *et al.*[15] controlled a single link flexible joint robot using proportional-integral-derivative (PID) and state feedback control algorithms. They compared the advantages and disadvantages of both control strategies and showed that both strategies give out similar results. Xue *et al.*[16] proposed using a discrete-time sliding mode controller coupled with an asynchronous sensor that estimates the future states. The proposed method seems to converge quickly to the desired trajectory; however they did not discuss the implications on the dynamics of the system or the sensitivity of the controller parameters.

Shabana[17] developed a generalized model of n-link serial robot including a number of flexible joints using multibody dynamics approach. A numerical algorithm is developed to simulate the obtained dynamic models in which Lagrange multipliers and numerical integration methods are implemented. Zaher[17] studied the effect of joints' flexibility on the dynamic performance of three-dimensional (3D) robots. The robot joint flexibility is represented by two spring-damper sets between the stator and the rotor of its drive and the rotor and the corresponding link. The contribution of this paper can be summarized into two points. The first contribution is the analysis of the effect of joints' flexibilities on the dynamic performance of a serial spatial robot arm compared to previous work in literature that utilizes either a single link robot or multilink planar robots. The second contribution is the development of a new model for the joint flexibility using standard multibody dynamics approaches. The use of this approach would enable the implementation of further flexibilities already researched in these approaches like contact formulations, damping and friction models, as well as spring nonlinearities. This paper is organized in six sections. After a literature survey in Section 1, Section 2 presents the basics of mathematical modeling. Section 3 presents the identification of links' inertial parameters and the joints flexibility coefficients of a three-link articulated robot with three flexible revolute joints. Section 4 presents the computation procedure and the simulation algorithm. Section 5 presents the obtained results with a brief discussion. The paper ends with some conclusions and recommendations in Section 6.

2. Mathematical Modeling of Constrained Dynamic Systems

2.1. Multibody dynamics approach

2.1.1. Equations of motion. Constrained dynamic systems are represented by (n_b) bodies/links and (n_c) kinematic constraints.[17,18] The Newtonian mechanics are used to develop the augmented formulation of the joints' kinematic constraint and the system dynamics can be represented in terms

https://doi.org/10.1017/S0263574714000848 Published online by Cambridge University Press

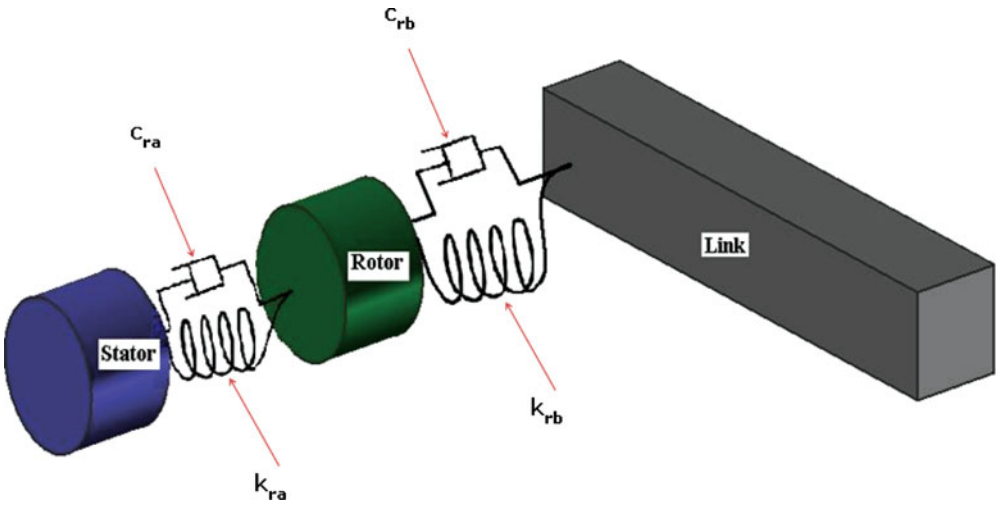

Fig. 1. General flexible joint.

of the Inverse Dynamic Model (IDM) as shown in Eq. (1) and the Direct Dynamic Model (DDM) as shown in Eq. (2).

$$\begin{bmatrix} \mathbf{M} & \mathbf{C}_\mathbf{q}^T \\ \mathbf{C}_\mathbf{q} & \mathbf{0} \end{bmatrix} \begin{bmatrix} \ddot{\mathbf{q}} \\ \lambda \end{bmatrix} = \begin{bmatrix} \mathbf{Q}_e + \mathbf{Q}_v \\ \mathbf{Q}_d \end{bmatrix}, \tag{1}$$

$$\begin{bmatrix} \ddot{\mathbf{q}} \\ \lambda \end{bmatrix} = \begin{bmatrix} \mathbf{M} & \mathbf{C}_\mathbf{q}^T \\ \mathbf{C}_\mathbf{q} & \mathbf{0} \end{bmatrix}^{-1} \begin{bmatrix} \mathbf{Q}_e + \mathbf{Q}_v \\ \mathbf{Q}_d \end{bmatrix}, \tag{2}$$

where

$\mathbf{M}$ is the body mass matrix $[6n_b \times 6n_b]$,
$\mathbf{q}$ is the vector of body generalized coordinates $[6n_b \times 1]$,
$\dot{\mathbf{q}}$ is the vector of body generalized velocities $[6n_b \times 1]$,
$\ddot{\mathbf{q}}$ is the vector of body generalized accelerations $[6n_b \times 1]$,
λ is the vector of Lagrange multipliers $[n_c \times 1]$,
$\mathbf{C}_q$ is the generalized Jacobian matrix of the kinematic constraints $[n_c \times 1]$,
$\mathbf{Q}_e$ is the vector of applied external generalized forces $[6n_b \times 1]$,
$\mathbf{Q}_d$ is the quadratic velocity vector that results from differentiation of the kinematic constraints equation twice with respect to time $[n_c \times 1]$,
$\mathbf{Q}_v$ is the quadratic velocity vector that results from differentiating the kinetic energy with respect to time and with respect to the generalized coordinates $[6n_b \times 1]$,
n_b is the number of bodies in the constrained system,
n_c is the number of kinematic constraints' equations.

2.1.2. Joints' constraints. Serial robots with revolute joints have two types of joint constraints, revolute and rigid joints constraints. The joints' constraints Jacobian matrix C_q is dependent on the type of the joint connection. The detailed formulation of the joint constraints equations are presented in refs. [17, 18].

2.1.3. Revolute joint flexibility model. The flexibility in a revolute joint exists at two locations (Fig. 1): first between the stator and the rotor and second between the rotor and the link. In case of a perfect revolute joint, $c_{ra} = 0$, $c_{rb} = 0$, $k_{ra} = 0$, and $k_{rb} = \infty$. Due to difficulty of estimation of all stiffness and damping coefficients simultaneously, the coefficients, c_{rb} and k_{rb} will be set as $c_{rb} = 0$ and $k_{rb} = \infty$ such that the joint flexibility is considered only between the stator and the rotor. Both values of the stiffness and damping coefficients range between zero and ∞. However, the exact values are unknown and need to be estimated:

https://doi.org/10.1017/S0263574714000848 Published online by Cambridge University Press

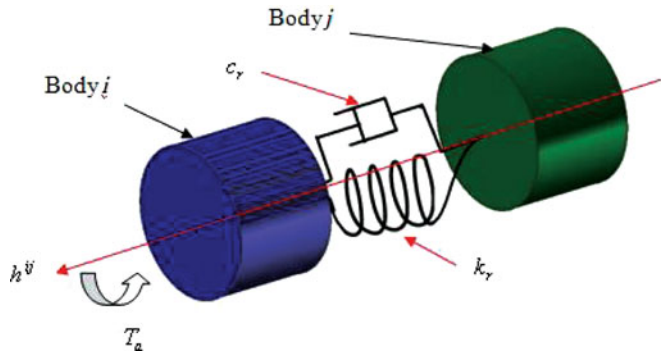

Fig. 2. Torsional spring damper actuator element.

- When k_r is set to zero, no spring exists between the two bodies.
- When k_r is set to infinity, the two bodies become one rigid body without relative rotation between them (rigid joint).
- When c_r is set to zero, no damping between the two bodies exists.
- When c_r equals infinity, no relative motion is allowed between the bodies it connects.

This flexibility may be represented by the standard element called Torsional Spring Damper Actuator (TSDA).[17–19] The TSDA element connects two bodies i and j in the multibody system and consists of three parts (Fig. 2):

1. torsional spring with stiffness coefficient k_r,
2. torsional damper with damping coefficient c_r,
3. actuator torque T_a.

Multibody dynamics approach deals only with forces acting on the bodies. The generalized external forces acting on the bodies are function of the resultant torque (T^{ji}) generated by the flexible joint. The torque exerted upon body (i) by the TSDA as a result of the rotation can be defined by Eq. (3).

$$T^{ji} = \left(k_r \beta^{ji} + c_r \dot{\beta}^{ji} + T_a\right), \tag{3}$$

where β^{ji} and $\dot{\beta}^{ji}$ are respectively, the relative rotational displacement and relative velocity of body j with respect to body i about the ith joint axis.

It can be shown that the relation between the infinitesimal rotation vector $\delta\pi^i$ about the axes of the global Cartesian coordinate system where $\omega^i = \delta\pi^i / \delta t$ and the virtual change in the generalized orientation coordinates $\delta\beta^i$ is given by Eqs. (4) and (5):[17–20]

$$\delta\pi^i = \mathbf{G}^i \delta\beta^i, \tag{4}$$

$$\mathbf{G}^i = \begin{bmatrix} 0 & \cos\varphi^i & \sin\theta^i \sin\varphi^i \\ 0 & \sin\varphi^i & -\sin\theta^i \cos\varphi^i \\ 1 & 0 & \cos\theta^i \end{bmatrix}. \tag{5}$$

Let $\mathbf{h}^{ij}$ be a unit vector along the joint axis. The virtual change in the angle of rotation between bodies i and j can be expressed in terms of the generalized orientation coordinates of the bodies i and j and is given by Eq. (6).

$$\delta\beta^{ji} = \mathbf{h}^{ijT}(\delta\pi^j - \delta\pi^i), \tag{6}$$

with $\delta\pi^i = \mathbf{G}^i \delta\beta^i$ and $\delta\pi^j = \mathbf{G}^j \delta\beta^j$. Using the principle of virtual work in terms of the virtual change in the generalized coordinates, as explained by Nada *et al.*,[19] the expressions of the generalized external forces Q^i and Q^j associated with the coordinates of the two jointed bodies i and j can be

https://doi.org/10.1017/S0263574714000848 Published online by Cambridge University Press

Table I. DH parameters and joint type indicator of the SRLFJ robot.

	1	2	3
σ_i	0	0	0
α_i (rad)	$\pi/2$	$-\pi/2$	0
a_i (m)	0	0.29	0.29
θ_i (rad)	q_1 (0)	q_2 (0)	q_3 (0)
r_i (m)	0.577	0	0

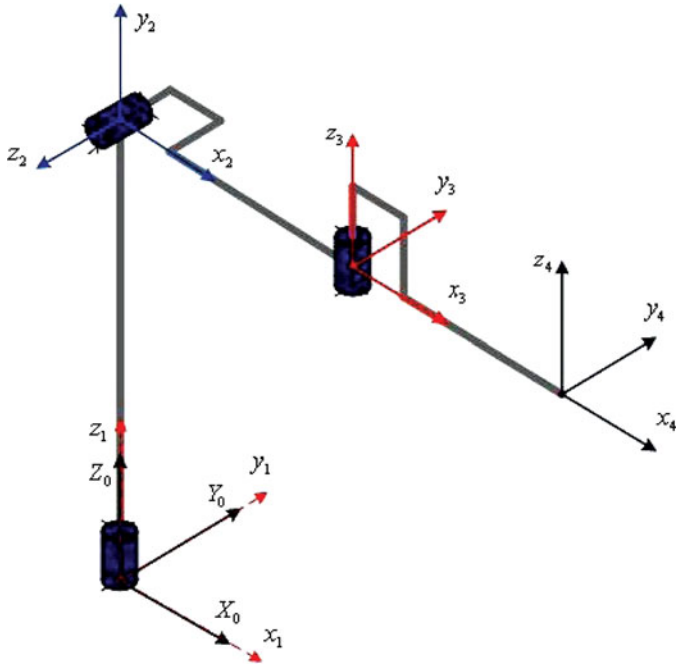

Fig. 3. SRLFJ robot kinematic diagram according to DH parameters.

obtained (Eqs. (7)–(9)).

$$\delta W = T^{ji}\delta\beta^{ji} = T^{ji}\mathbf{h}^{ijT}(\delta\pi^j - \delta\pi^i), \tag{7}$$

$$\delta W = \mathbf{Q}^{jT}\delta\mathbf{q}^j - \mathbf{Q}^{iT}\delta\mathbf{q}^i, \tag{8}$$

$$\mathbf{Q}^i = \begin{bmatrix} \mathbf{0} \\ T^{ji}\mathbf{G}^{iT}\mathbf{h}^{ij} \end{bmatrix}, \quad \mathbf{Q}^j = \begin{bmatrix} \mathbf{0} \\ T^{ji}\mathbf{G}^{jT}\mathbf{h}^{ij} \end{bmatrix}. \tag{9}$$

2.2. Robotics approach

The classical robotics modeling approach is selected to develop a model for the robot with joint damping as it proved its usefulness for many years. This section describes the basis of mathematical modeling of robots. The spatial rigid link flexible joint (SRLFJ) robot kinematic model (Fig. 3) can be represented by the Denavit–Hartenberg (DH) parameters with Euler angles (*Z–X–Z*; Table I). While this kinematic model does not account for joint flexibility, it will be assumed that the joint flexibility effects will take place in the dynamic model. The robot dynamic models can be obtained using Euler–LaGrange and the Recursive Newton–Euler (RNE) formulations.

The inverse (IDM) and direct dynamic models (DDM) can be represented in Lagrangian formulation by Eqs. (10) and (11), respectively.[21]

$$\Gamma(q, \dot{q}, \ddot{q}, \gamma) = E_a\ddot{q} + 2E_b\dot{q}\dot{q} + E_c\dot{q}^2 - E_g + E_p, \tag{10}$$

https://doi.org/10.1017/S0263574714000848 Published online by Cambridge University Press

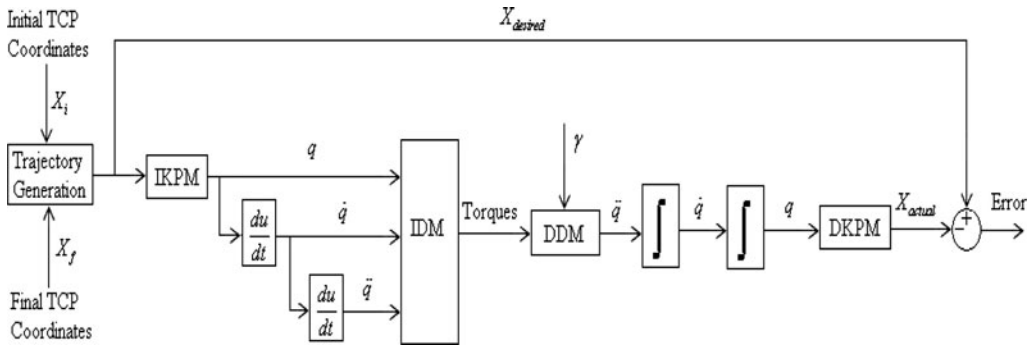

Fig. 4. Computational procedure block diagram (from ref. [22]).

$$\ddot{q} = E_a^{-1}\left(\Gamma\left(q, \dot{q}, \ddot{q}, \gamma\right) - 2E_b\dot{q}\dot{q} - E_c\dot{q}^2 + E_g - E_p\right), \tag{11}$$

where

E_a is the kinetic energy symmetric matrix [$6n_b \times 6n_b$],
E_b is a [$6n_b \times 6n_b$ (n_b+1)/2] matrix representing Coriolis acceleration effects,
E_c is a [$6n_b \times 6n_b$] matrix representing the centrifugal force effects,
E_g is a vector representing the gravity forces coefficients [$6n_b \times 1$],
E_p is the vector of perturbation forces [$6n_b \times 1$], and
n_b is the number of links in the robot.

As the presence of the damper causes energy losses, the equation representing the actual driving torques in flexible joint robots needed to be modified to account for these losses as shown in Eq. (12).

$$\Gamma = \Gamma\left(q, \dot{q}, \ddot{q}, \gamma\right) - c_r\dot{q}, \tag{12}$$

where

Γ is the generalized torque acting on the joint,
$\Gamma\left(q, \dot{q}, \ddot{q}, \gamma\right)$ is the computed torque acting on the perfect joint,
γ is the term that includes the robot inertias and center of gravity coordinates,
c_r is the rotational damping coefficient,
q is the joint angle,
$\dot{q}$ is the joint angular velocity,
$\ddot{q}$ is the joint angular acceleration.

The obtained dynamic models are used to develop a numerical algorithm. The following steps are used for simulating the dynamic behavior of any robot (Fig. 4):

1. planning and generation of the desired tool center point (TCP) trajectory (X_{desired}),
2. inverse kinematics position model (IKPM),
3. IDM,
4. DDM,
5. integrating the joints' angular accelerations and minimizing the integration error to get the angular velocities and displacements,
6. direct kinematics position model (DKPM), and
7. comparing the desired trajectory with the actual one.

3. Estimation of Robot Inertial and Flexibility Parameters

The SRLFJ robot is developed using the computer-aided design (CAD) NX, taking into consideration the practical data of the available materials and components (Fig. 5).[22] Also, it is used to determine the robot inertial parameters, locations of links' centers of gravity and the joints' coordinates data (Table II). The mass is verified by weighing the SRLFJ robot. Since the identification of the accurate values for the joints' damping coefficients is not the focus of this paper, estimated values are used.

https://doi.org/10.1017/S0263574714000848 Published online by Cambridge University Press

Table II. Inertial parameters of the SRLFJ links.

Body	Mass (kg)	I_{xx} (kg m^2)	I_{yy} (kg m^2)	I_{zz} (kg m^2)	I_{xy} (kg m^2)	I_{xz} (kg m^2)	I_{yz} (kg m^2)
Link 1	3.136	1.406E-1	2.01E-2	1.28E-1	−7.9E-3	−3.95E-3	2.04E-2
Link 2	6.202	2.51E-2	1.3E-1	1.13E-1	5.36E-5	1.21E-2	2.18E-5
Link 3	0.412	1.41E-4	4.05E-3	3.92E-3	−2.5E-5	−1.37E-5	2.45E-7

Table III. SRLFJ robot BFC position and orientation.

Body name		R_{xi} (m)	R_{yi} (m)	R_{zi} (m)	φ^i(rad)	θ^i(rad)	ψ^i(rad)
Ground	Body 1	0	0	0	0	0	0
Link 1	Body 2	−0.0185	0.043	0.376	0	$\pi/2$	0
Link 2	Body 3	0.00044	0.00323	0.5837	0	0	0
Link 3	Body 4	0.3895	0.0012	0.5713	0	0	0

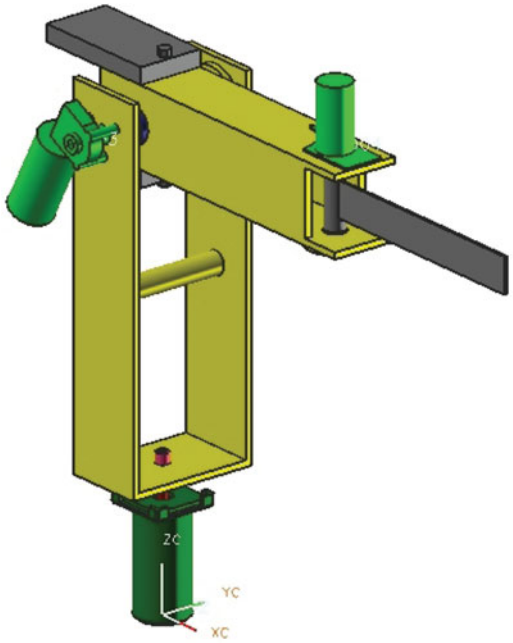

Fig. 5. SRLFJ robot CAD model.

The first and the second links are made of acrylic, with the exception of the actuators and the joint components. The second link has two counterbalance iron masses of 2.15 kg each to adjust the center of mass of the second link closer to the joint center. This reduces the driving torques, hence decreasing the power requirements to drive the robot. The third link is a steel beam.

Table III gives the SRLFJ robot bodies fixed coordinates (BFC) position and orientation using Cartesian coordinates and Euler angles (Fig. 6). All body forces are neglected and the initial velocities are equal to zero.

3.1. Estimation of joints' flexibility coefficients

Estimation of the joints' parameters is needed for the experimental verification process (Fig. 7). A modified flexible joint model (Fig. 8) is developed based on the simulation results which will be discussed in the paper. The joints' flexibility is a direct result of many sources such as flexible elements assumed rigid (shafts, gears), lubrication, friction, flux losses, gyroscopic effect, and other miscellaneous sources. Among these sources are the gear teeth compliance and the motor shaft stiffness which are considered in this section. Since the finite element analysis of helical gears to evaluate their compliances is not within the scope of this work, a more basic approach is used to

https://doi.org/10.1017/S0263574714000848 Published online by Cambridge University Press

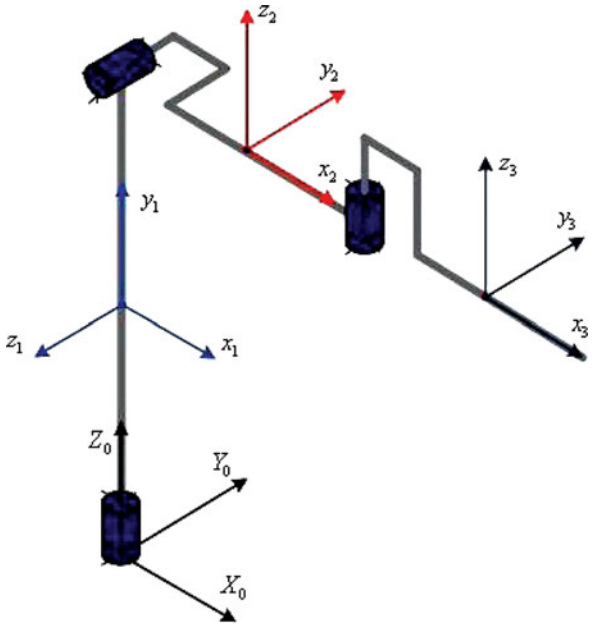

Fig. 6. SRLFJ robot kinematic diagram with multibody BFCs.

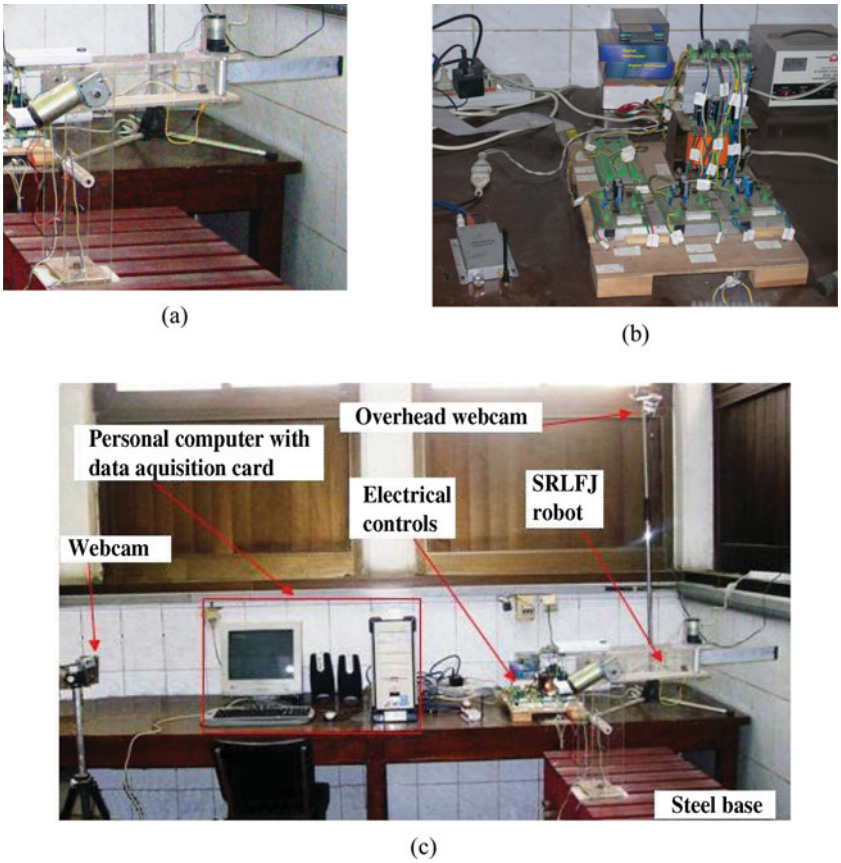

Fig. 7. Modular SRLFJ robot.

https://doi.org/10.1017/S0263574714000848 Published online by Cambridge University Press

Table IV. Data and computations for the first flexible joint.

Body	$D = 2r$ (mm)	Ψ (deg)	b (mm)	h (mm)	L (mm)	I (mm^4)	k (Nm/rad)
Gear 1	7	18	4	1.35	1.5	1.845	1340
Gear 2	32.5	18	4	1.35	1.5	1.845	28,871
Gear 3	11	9	6	1.35	1.5	1.23	2204
Gear 4	45	9	6	1.35	1.5	1.23	36,900
Shaft	10	–	–	–	62	981.75	1267

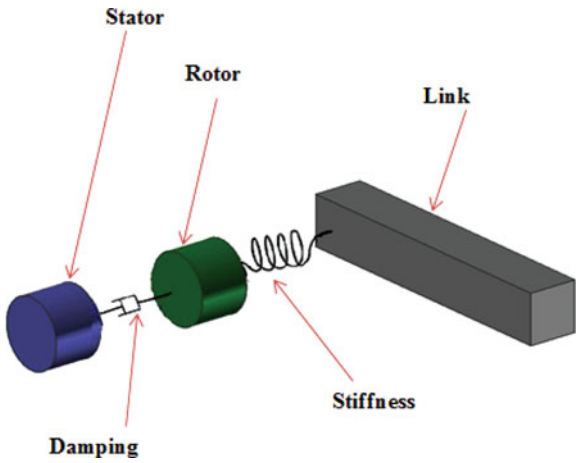

Fig. 8. Modified flexible joint.

approximately estimate the stiffness coefficients of helical gears and their contribution to the joint stiffness. The gears and motor shaft parameters were obtained from the hardware components. Some assumptions are made to assist in this stiffness estimation:

1. The flexible joint stiffness coefficients are results of the gears and shafts only.
2. Gear teeth are assumed to be cantilever beams.
3. The rotational stiffness of the gear tooth is equal to that of the cantilever beam multiplied by square the gear radius. This basic approach is used for simplicity as a preliminary method of estimation.
4. All gears and shafts are made of steel with $E = 207$ GPa and $G = 84$ GPa.
5. The system is a group of springs in series.

The gear stiffness coefficient values are estimated using traditional cantilever beam equation and the mass moment of inertia of the rotor shafts. Table IV provides the data and the results for the first flexible joint.

The estimation of joints' damping coefficients is more complex. The lubricants' viscosity varies with changes in both temperature and speed. Eschmann *et al.*[23] provided the empirical procedures for the damping coefficients estimation in rolling contact bearings. To estimate the joints' damping coefficients the following assumptions are taken into consideration:

1. A flexible joint damping coefficient is a result of the bearings only.
2. All damping coefficients are motor referred.
3. The bearing holding the worm gear is not taken into consideration.
4. No power losses in the gearbox.
5. Gear traverse pressure angle is 20°.

The detailed estimation process is presented in Zaher's thesis,[18] and the procedure is explained in Eschmann *et al.*[23] Video processing techniques via low resolution cameras are used to record the experimental results. Tables V–XIII present the data used as inputs to the simplified model. The driving torques are applied as moments on the rotors.

https://doi.org/10.1017/S0263574714000848 Published online by Cambridge University Press

Table V. SRLFJ robot local coordinates of the 1st point on the revolute joints' axes.

			Local coordinates of the 1st point on					
			Body i (m)			Body j (m)		
Joint #	1st body i	2nd body j	X_{i1}	Y_{i1}	Z_{i1}	X_{j1}	Y_{j1}	Z_{j1}
1	1	2	0	0	0	0.0185	−0.376	−0.043
2	2	3	0.0189	0.2007	–0.00528	0	0	0
3	3	4	0.29	0	0	−0.109	0	0

Table VI. SRLFJ robot local coordinates of the 2nd point on the revolute joints' axes.

			Local coordinates of the 2nd point on					
			Body i (m)			Body j (m)		
Joint #	1st body i	2nd body j	X_{i2}	Y_{i2}	Z_{i2}	X_{j2}	Y_{j2}	Z_{j2}
1	1	2	0	0	1	0.0185	0	−0.043
2	2	3	0.0189	0.2007	1	0	−1	0
3	3	4	0.29	0	1	−0.109	0	1

Table VII. TSDA's axes coordinates of the SRLFJ robot.

			Local coordinates of two points along the element axis on Body i (m)					
TSDA #	1st body i	2nd body j	X_{i1}	Y_{i1}	Z_{i1}	X_{i2}	Y_{i2}	Z_{i2}
1	1	2	0	0	0	0	0	1
2	2	3	0.0189	0.2007	−0.00528	0.0189	0.207	1
3	3	4	0.29	0	0	0.29	0	1

Table VIII. Inertial parameters of the new model.

Body	Mass (kg)	I_{xx} (kg m^2)	I_{yy} (kg m^2)	I_{zz} (kg m^2)	I_{xy} (kg m^2)	I_{xz} (kg m^2)	I_{yz} (kg m^2)
Ground	100	100	100	100	100	100	100
Rotor 1	0.656	1.053E-3	6.94E-5	1.05E-3	1.16E-5	−1.3E-7	−1.12E
Link 1	2.289	6.916E-2	2.20E-2	5.02E-2	3.63E-4	−7.17E-5	1.47E-2
Rotor 2	0.656	1.053E-3	6.94E-5	1.05E-3	1.25E-5	−1.4E-7	−1.13E-5
Link 2	6.24	2.5495E-2	1.34E-1	1.12E-1	−1.2E-3	1.04E-2	8.36E-5
Rotor 3	0.005	3.9E-7	3.9E-7	1.5E-8	5.0E-11	4.0E-9	4.0E-9
Link 3	0.411	1.337E-4	4.02E-3	3.90E-3	−7.68E-5	−3.54E-5	2.03E-6

Table IX. Position and orientation of the reference frames.

Body name		R_{xi} (m)	R_{yi} (m)	R_{zi} (m)	φ^i (rad)	θ^i (rad)	ψ^i (rad)
Ground	Body 1	0	0	0	0	0	0
Rotor 1	Body 2	0.00077	0.001733	0.06469	0	$\pi/2$	0
Link 1	Body 3	0.00478	−0.05534	0.47136	0	$\pi/2$	0
Rotor 2	Body 4	0.00478	−0.15272	0.57875	0	0	0
Link 2	Body 5	0.00918	0.01032	0.5832	0	0	0
Rotor3	Body 6	0.29729	0.0073	0.615	0	0	0
Link 3	Body 7	0.4049	0.00354	0.57109	0	0	0

https://doi.org/10.1017/S0263574714000848 Published online by Cambridge University Press

Table X. TSDA's damping and stiffness coefficients.

Joint	1		2		3	
TSDA #	1	2	3	4	5	6
c_r	2.36E-5	0	1.325E-5	0	6.5E-6	0
k_r	0	488	0	503	0	67

Table XI. Local coordinates of the 1st point on each body for revolute joints axes.

			Local coordinates of the 1st point on					
			Body i (m)			Body j (m)		
Joint #	1st body i	2nd body j	X_{i1}	Y_{i1}	Z_{i1}	X_{j1}	Y_{j1}	Z_{j1}
1	1	2	5E-5	1.03E-3	2.99E-3	−7.2E-4	−0.0617	7E-4
2	2	3	1.48E-3	0.1253	−1.42E-3	−2.53E-3	−0.2814	−0.0585
3	3	4	−7.9E-4	0.1081	0.1591	−7.9E-4	−0.0617	7.1E-4
4	4	5	1.58E-3	0.1253	−1.44E-3	−2.82E-3	−0.0377	−5.9E-3
5	5	6	0.2892	−2.0E-3	0.1223	1.06E-3	1.03E-3	9.05E-2
6	6	7	−1.9E-4	−1.8E-4	−0.0155	−0.1078	3.59E-3	2.84E-2

Table XII. Local coordinates of the 2nd point on each body for revolute joints axes.

			Local coordinates of the 2nd point on					
			Body $\underline{i}$ (m)			Body j (m)		
Joint #	1st body i	2nd body j	X_{i2}	Y_{i2}	Z_{i2}	X_{j2}	Y_{j2}	Z_{j2}
1	1	2	2.25E-3	3.15E-3	0.190	1.48E-3	0.1253	−1.42E-3
2	2	3	5.7E-4	4.83E-2	−5.5E-4	−3.44E-3	−0.3584	00.0576
3	3	4	6.1E-4	0.1068	0.0491	6.1E-4	0.0483	−5.5E-4
4	4	5	6.1E-4	4.83E-2	−5.5E-4	−0.0038	−0.1148	−5E-3
5	5	6	0.2882	−2.9E-3	0.0423	1.2E-4	1.2E-4	0.0105
6	6	7	1.2E-4	1.2E-4	0.0105	−0.1075	3.88E-3	0.05441

Table XIII. TSDAs axes coordinates.

			Local coordinates of two points along the element axis on body i (m)					
TSDA #	1st body i	2nd body j	X_{i1}	Y_{i1}	Z_{i1}	X_{i2}	Y_{i2}	Z_{i2}
1	1	2	5E-5	1.03E-3	2.99E-3	2.25E-3	3.15E-3	0.190
2	2	3	1.48E-3	0.1253	−1.42E-3	5.7E-4	4.83E-2	−5.5E-4
3	3	4	−7.9E-4	0.1081	0.1591	6.1E-4	0.1068	0.0491
4	4	5	1.58E-3	0.1253	−1.44E-3	6.1E-4	4.83E-2	−5.5E-4
5	5	6	0.2892	−2.0E-3	0.1223	0.2882	−2.9E-3	0.0423
6	6	7	−1.9E-4	−1.8E-4	−0.0155	1.2E-4	1.2E-4	0.0105

4. Computation Procedure and Simulation Algorithm

Robots are used to perform certain tasks in a certain time span. To perform these tasks, the TCP of a robot end-effector must follow a certain path or trajectory in space. Hence, a trajectory generation technique using spline functions is used by Megahed[22] to determine the global coordinates, velocities, and accelerations of the robot TCP along the desired path for the desired time span. Hence, the joints' angles coordinates can be calculated using the inverse kinematics as explained by Zaher[18] and Megahed.[22] The orientations of the links are chosen such that the joint angle coincides with one of the Euler angles of the link driven by the joint. Selecting the orientations in such manner allows for

https://doi.org/10.1017/S0263574714000848 Published online by Cambridge University Press

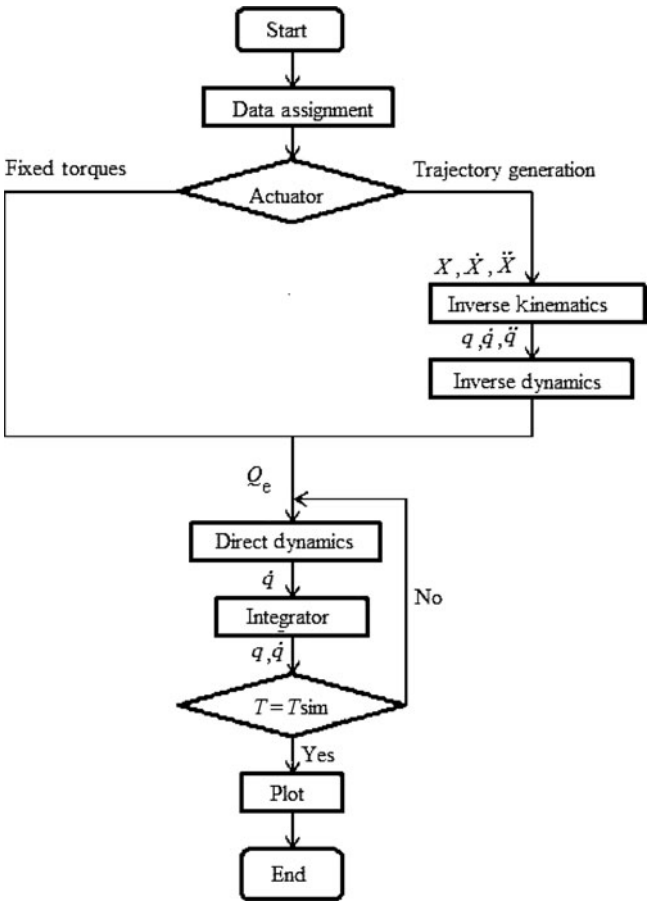

Fig. 9. Flowchart of the multibody Code.

the calculation of the generalized forces and coordinates using the IDM and the DDM (Eqs. (1) and (2)) respectively (Fig. 9). Through comparison and solving, it can be shown that actual orientation of the TCP of the SRLFJ robot using Euler angles (*Z*–*X*–*Z*) can be written in terms of the joints' angles (Eq. (13)).

$$\left.\begin{aligned} \phi &= q_1 - \frac{\pi}{2} \\ \theta &= q_2 \\ \psi &= q_3 + \frac{\pi}{2} \end{aligned}\right\}. \tag{13}$$

The robot TCP desired trajectory is selected as a straight line based on the ideal case robot. A spline trajectory is outlined in analytical form[22] such that all velocities and accelerations start and end to rest. The initial and final positions of the robot's TCP are:

- Initial positions robot joints angles (0°, 0°, 0°) and the Cartesian global coordinates of the TCP adjacent to these joint angles are (0.58, 0, 0.577) meters.
- Final positions of robot joints angles (–145°, 45°, 80°) and the adjacent Cartesian global coordinates of the TCP of these angles are (–0.0333, –0.3720, 0.8177) meters.
- The desired execution time is set to be 5 s.

Figures 10–12 show the joints states for the desired trajectory of the ideal robot. Figures 13 and 14 show the desired trajectory coordinates and orientations of the ideal robot. The driving torques are obtained using the robotics methodology. Using curve fitting code, the torque polynomials can be obtained. Figures 15–17 show the smoothed driving torques curves for the desired trajectory. The Newton–Raphson iterations are used with a limit of 1000 iterations. The absolute error tolerance is

https://doi.org/10.1017/S0263574714000848 Published online by Cambridge University Press

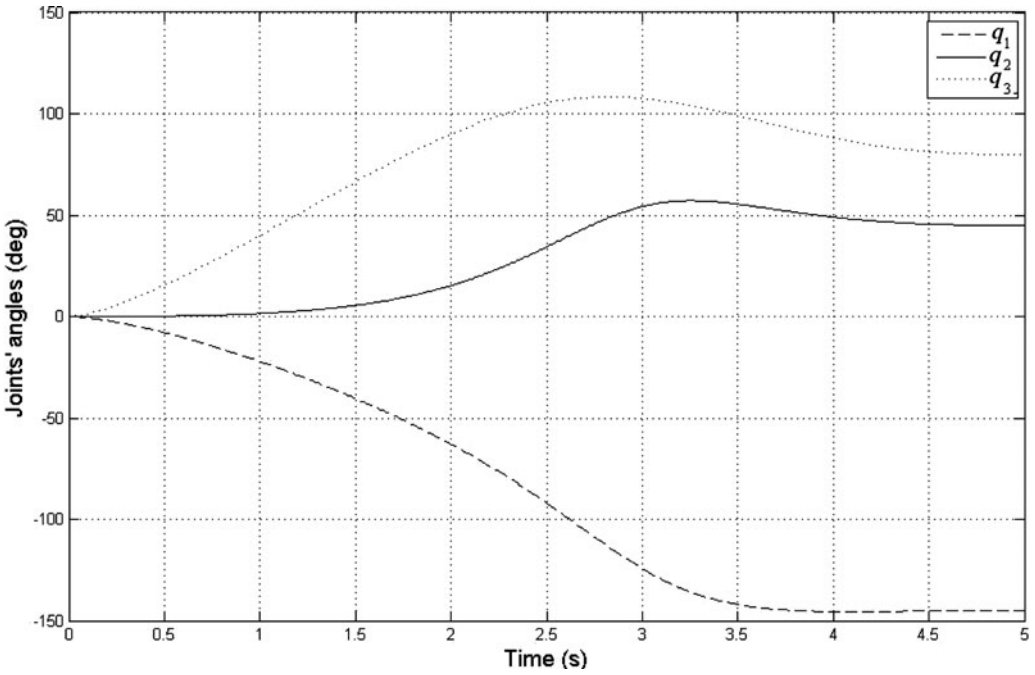

Fig. 10. Trajectory joints angles of the SRLFJ robot.

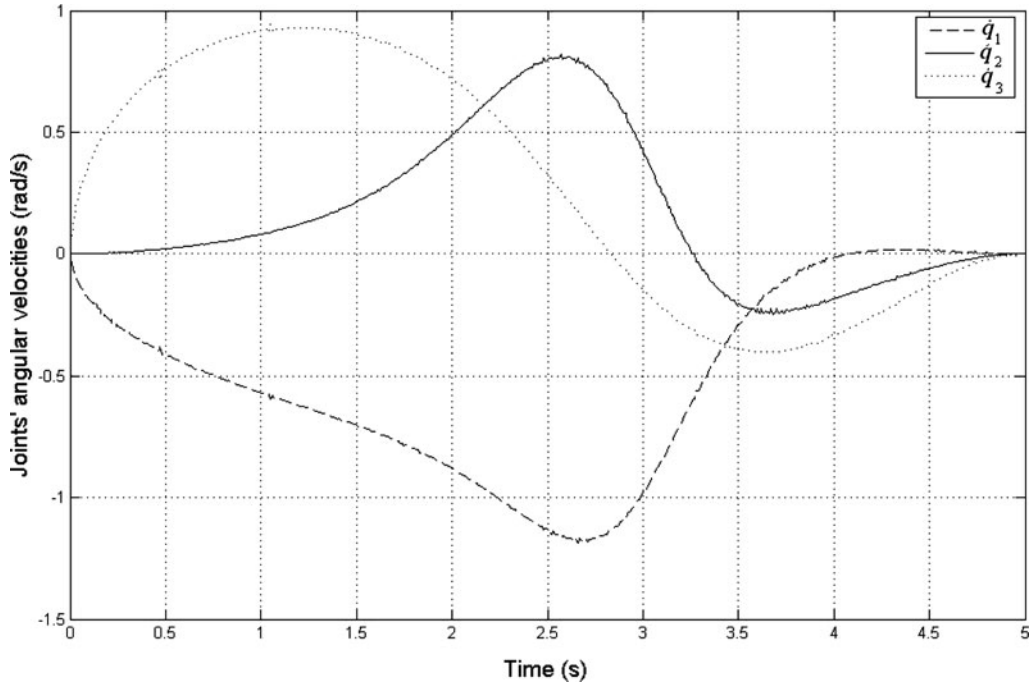

Fig. 11. Trajectory joints angular velocities of the SRLFJ robot.

set to 1E-6. Adams integrator and the fixed step integrator Explicit Runge–Kutta (Dormand–Prince) methods are used with this model.

5. Simulation and Experimentation

The simulations are conducted in three phases. In the first phase, the modified generalized joint model is used. This phase resulted in the elimination of the joint stiffness between the stator and the rotor. In

https://doi.org/10.1017/S0263574714000848 Published online by Cambridge University Press

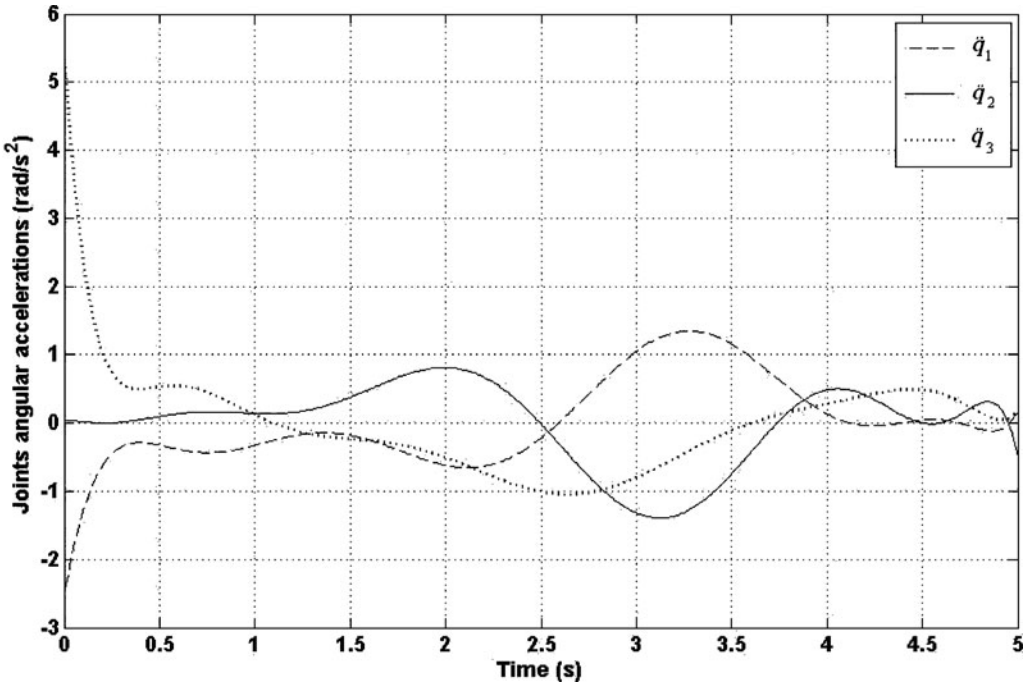

Fig. 12. Trajectory joints angular accelerations of the SRLFJ robot.

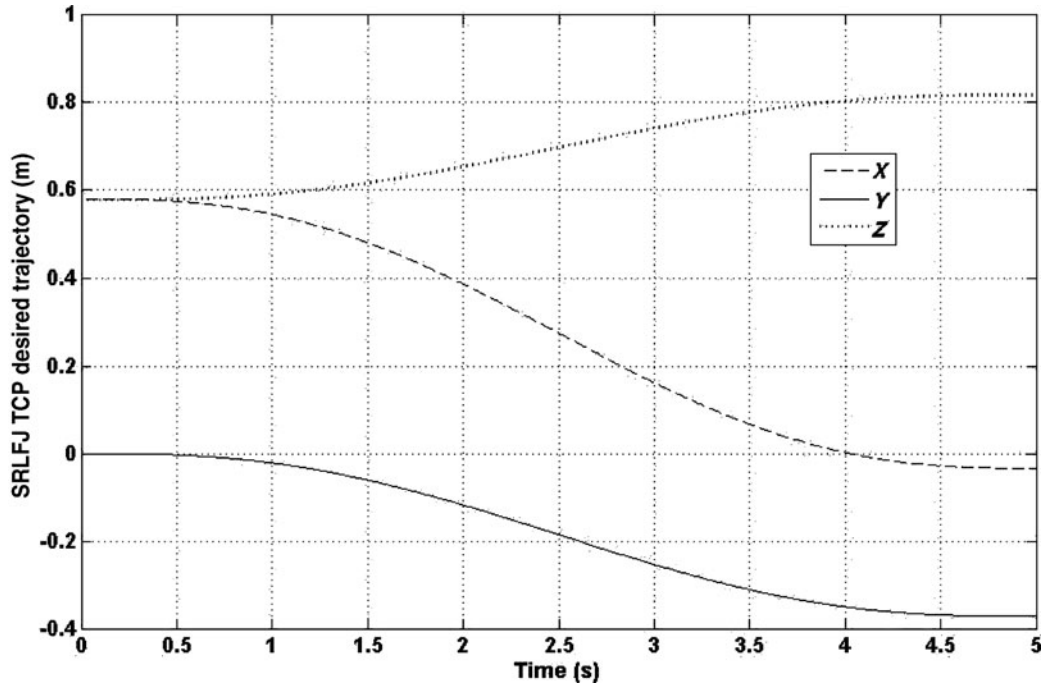

Fig. 13. SRLFJ robot TCP desired trajectory coordinates.

the second phase, a parametric study was conducted over a random logarithmic range for the effect of the damping on the positioning error. The third and final phase used the modified model deducted from the results of the previous phases and the estimated empirical parameters were used. The results from the third phase and the experimental setup have been compared.

https://doi.org/10.1017/S0263574714000848 Published online by Cambridge University Press

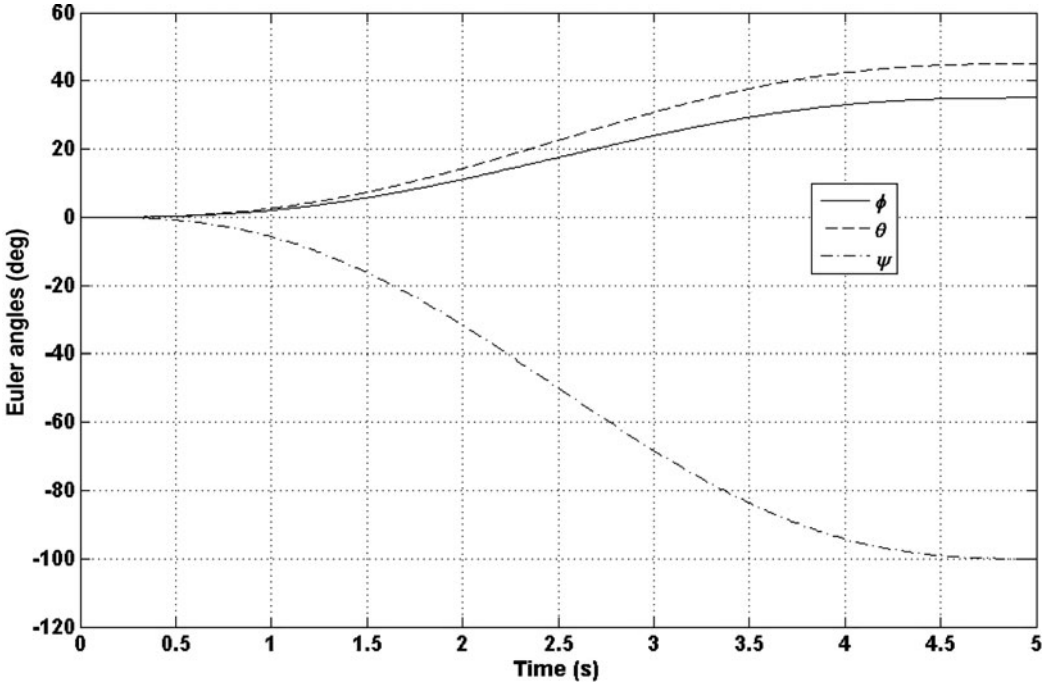

Fig. 14. SRLFJ robot TCP desired trajectory orientations.

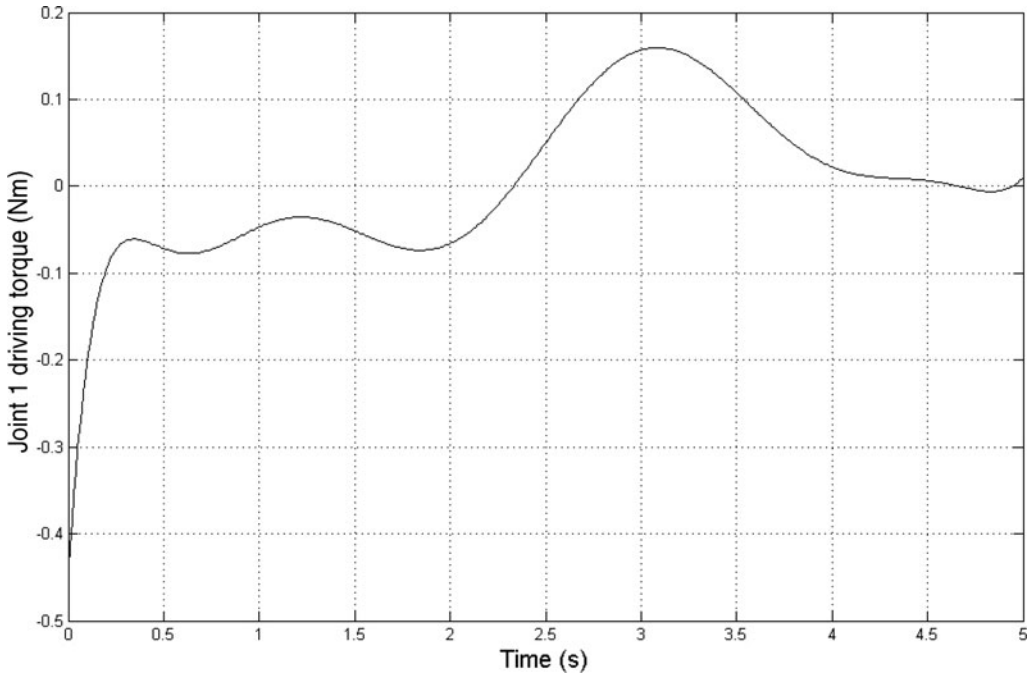

Fig. 15. Driving torque of the first joint.

5.1. Elimination of the stator-rotor stiffness

The absolute difference of the TCP position from the ideal case is obtained by the calculating the norm of total Cartesian deviations. For this reason, the coefficients' values are selected via trial and error such that the maximum absolute TCP error from the ideal case does not exceed ± 1 mm which is a high accuracy specification for industrial robots. Through random iterations over the log scale; the values of the coefficients have been tested. Figure 18 demonstrates that for very small values of spring stiffness coefficients between the stator and the rotor, the SRLFJ robot's TCP will miss its

https://doi.org/10.1017/S0263574714000848 Published online by Cambridge University Press

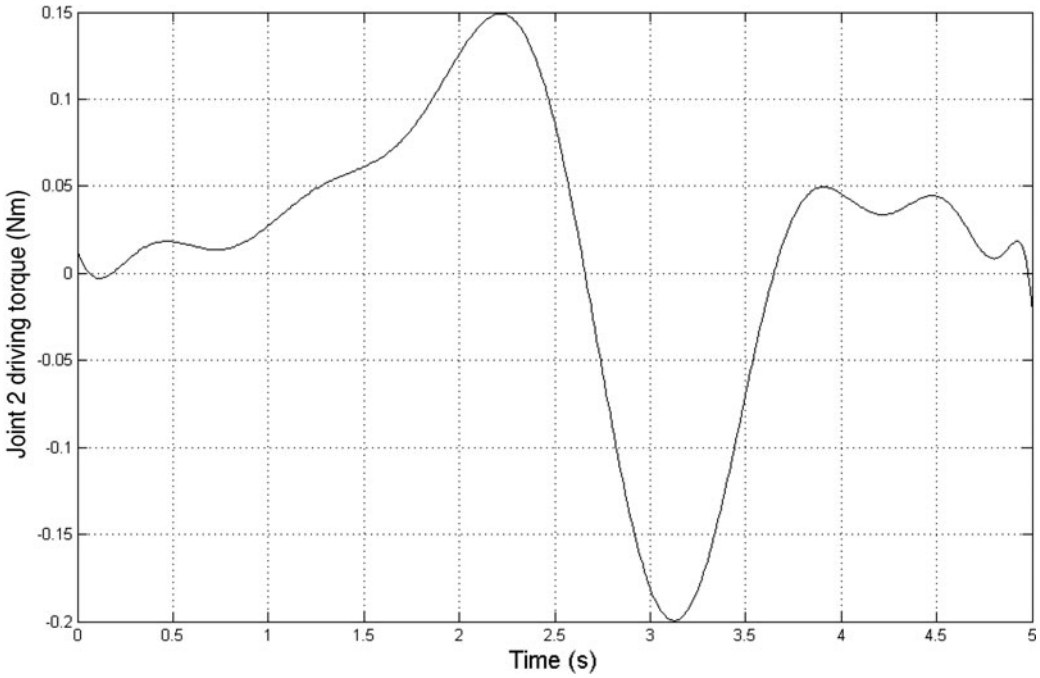

Fig. 16. Driving torque of the second joint.

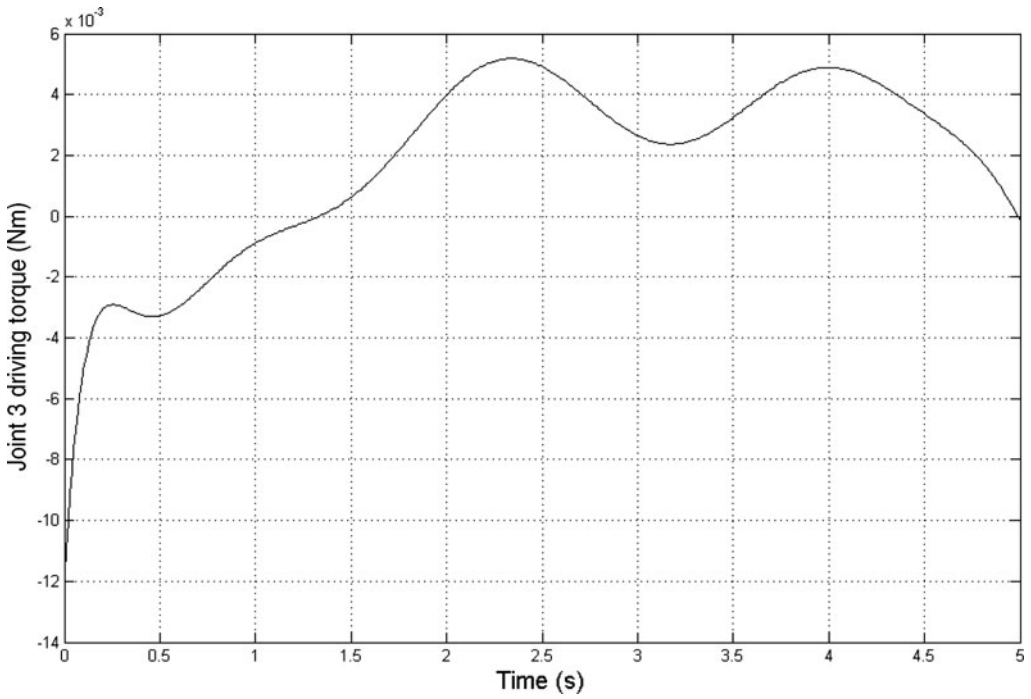

Fig. 17. Driving torque of the third joint.

desired location by over 30 mm. Because real joint stiffness coefficients are of much higher values, It is concluded that the spring stiffness between the stator and the rotor cannot physically exist (i.e. $k_r = 0$ Nm/rad). Hence, spring stiffness can only exist between the rotor and the link. This allows for the development of the new modified model containing only stiffness between the rotor and the link and a damping between the stator and the rotor (Fig. 8).

https://doi.org/10.1017/S0263574714000848 Published online by Cambridge University Press

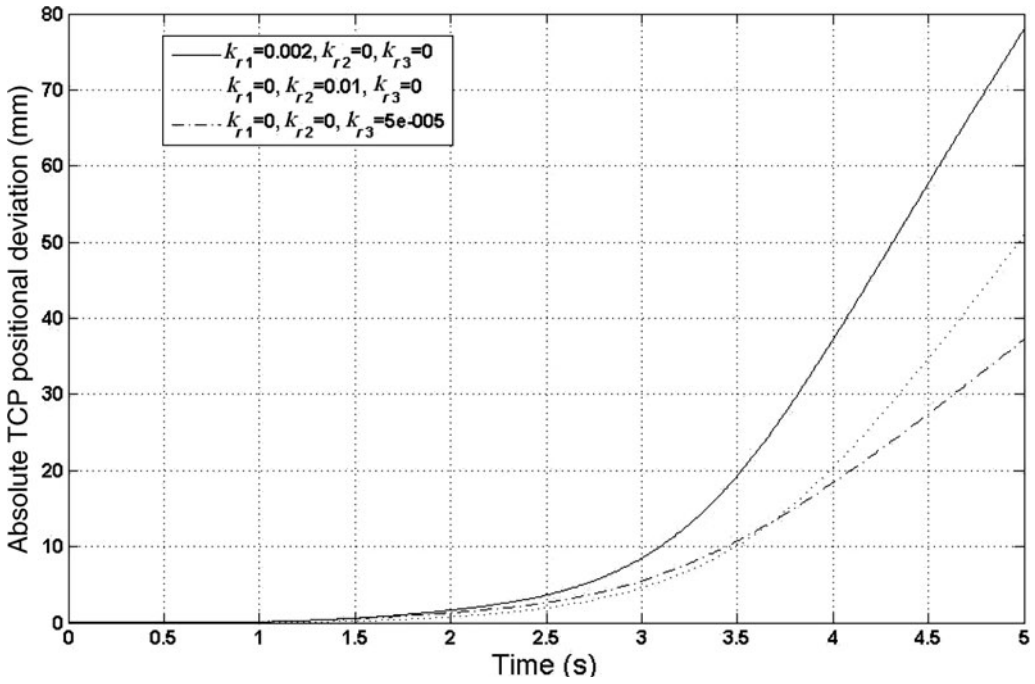

Fig. 18. Effect of joint stiffness between the stator and the rotor on the TCP position.

5.2. Parametric study on the damping effect

Figure 19 presents the effect of the damping coefficient of the first joint on the absolute TCP position deviation relative to that of the ideal case. The damping of the first joint causes the TCP to deviate accumulatively from the perfect case. It is noticed that for the highest selected value of c_{r1}, the error decreases when c_{r3} is set to a value other than zero. This implies that it is possible to use the other joints to compensate for the deviation caused by the first joint. From Figs. 19–21, it can be deduced that the effect of the joint damping coefficients c_{r1}, c_{r2} and c_{r3} on the robot TCP positioning is dependent on both the value and the location of the damping. It can be noted that the effect of c_{r1} is the highest; and that effect of c_{r3} on the deviation is higher than c_{r2}. Figure 22a shows that for low values of c_{r1}, the damping effect on the TCP position tends to be negligible as the other damping values act as the dominant parameters. However, when c_{r1} is set to a higher value, it starts to affect the TCP position leading it to become closer to the ideal target point, even though the trajectory tends to be wavy around that caused by the other damping coefficients. Figure 22b shows that for low values of c_{r2}, the damping effect on the TCP position tends to be negligible as the other damping values act as the dominant parameters. However, when c_{r2} is set with a higher value, it starts to affect the TCP position leading it to become closer to the ideal target point. Also, it decreases the overall deviation at all points along the selected trajectory. Figure 22c shows that for low values of c_{r3}, the damping effect on the TCP position tends to be relatively small, while the other damping values act as the dominant parameters. However, the higher the value of c_{r3}, the closer the TCP follows the trajectory of the ideal case.

Also, for the high value of c_{r3}, an overcrossing between curves occurs which can be related to the individual coordinates' deviations occurring as seen from Fig. 23. While the deviation in some coordinates is large for certain damping coefficient values, for these same values the deviation could be small.

5.3. Experimental verification

The experimental results give TCP coordinates similar to that of the perfect joint robot (Fig. 24), however, the simulation with the new model provides entirely different results. For instance it is noticeable that the *Z*-axis of the simulated results moves in the opposite direction to the expected results. This is attributed to the presence of multiple possible solutions for an IDM model which cannot be controlled without adding geometrical constraints on the motion. It is noticed that the

https://doi.org/10.1017/S0263574714000848 Published online by Cambridge University Press

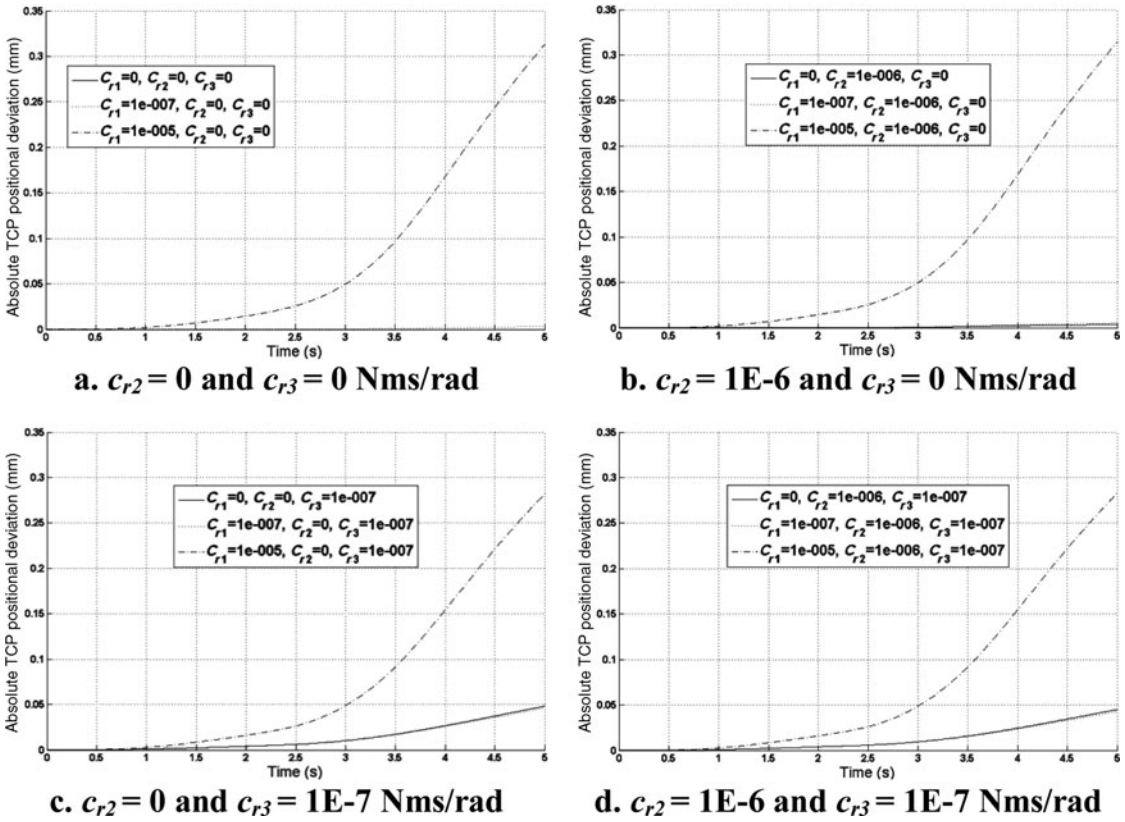

Fig. 19. Parametric study of the effect of c_{r1} on the TCP position.

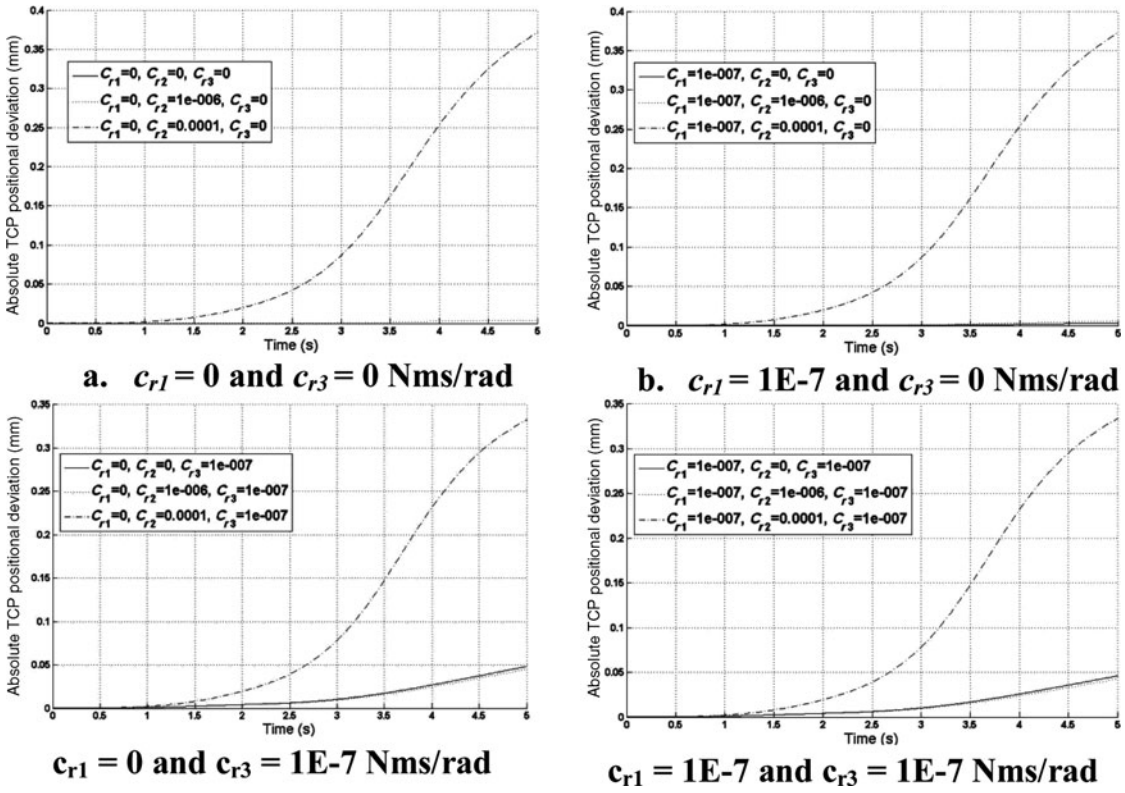

Fig. 20. Parametric study of the effect of c_{r2} on the TCP position.

https://doi.org/10.1017/S0263574714000848 Published online by Cambridge University Press

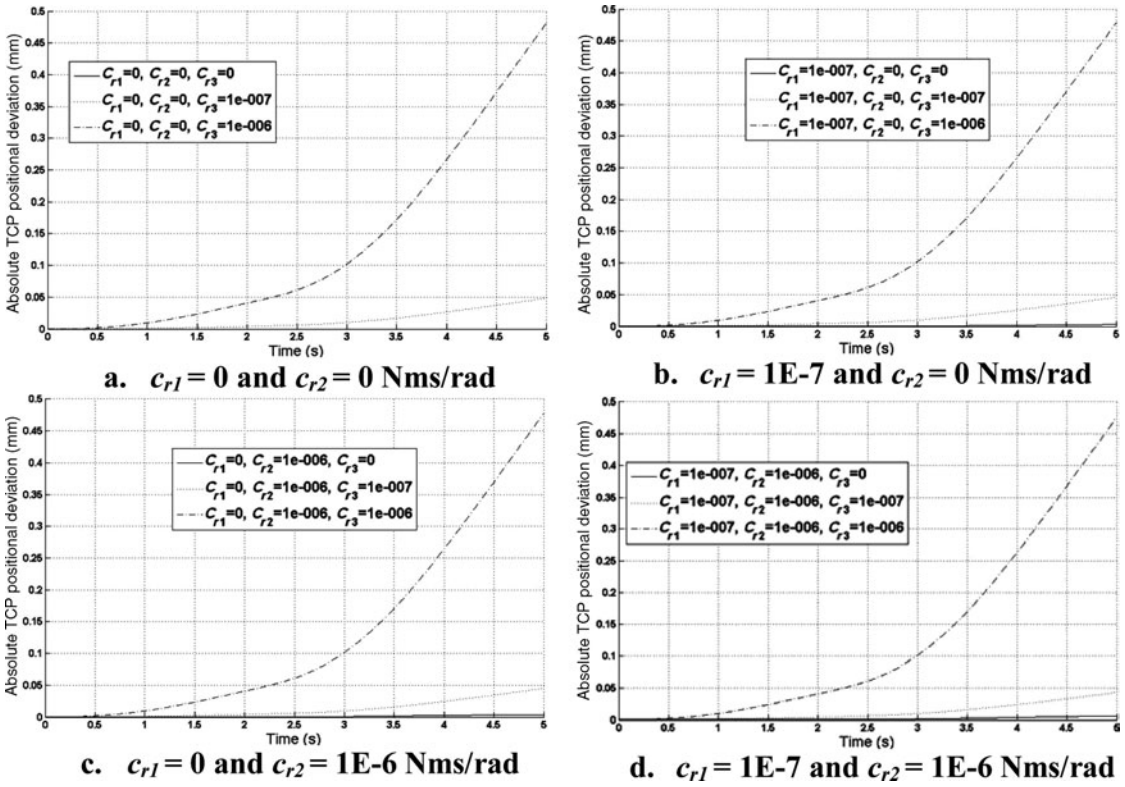

Fig. 21. Parametric study of the effect of c_{r3} on the TCP position.

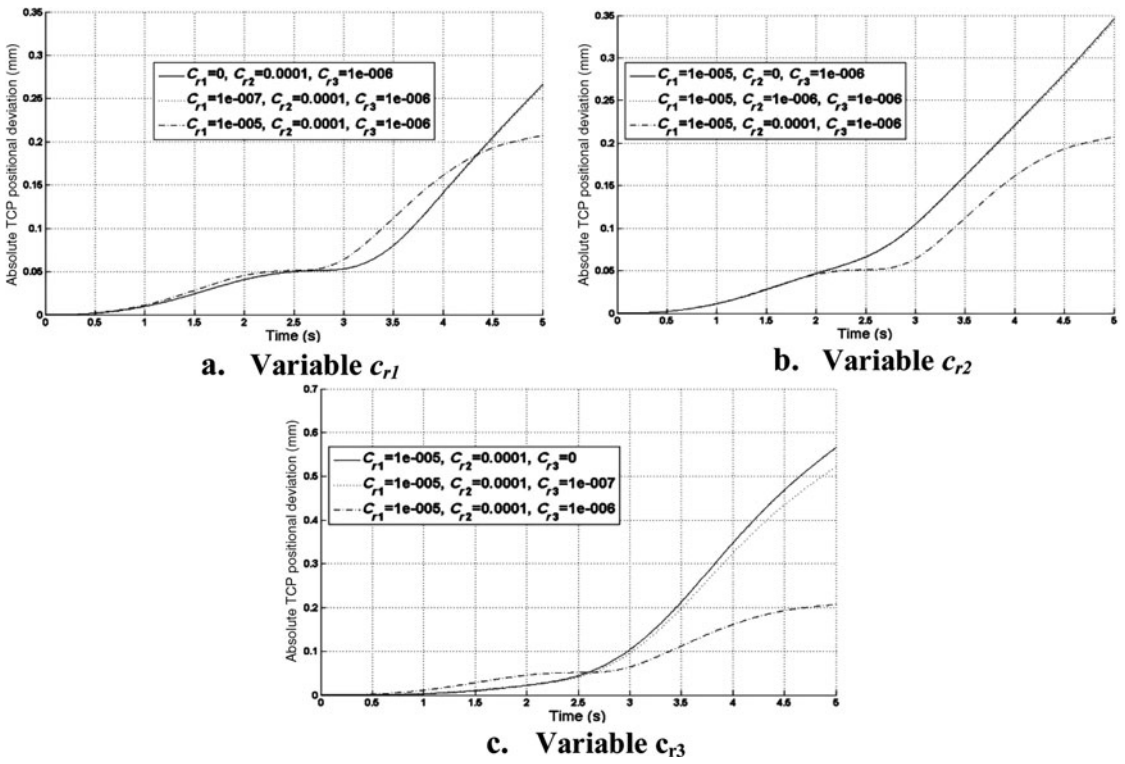

Fig. 22. Effect of the high damping coefficient values on the TCP.

https://doi.org/10.1017/S0263574714000848 Published online by Cambridge University Press

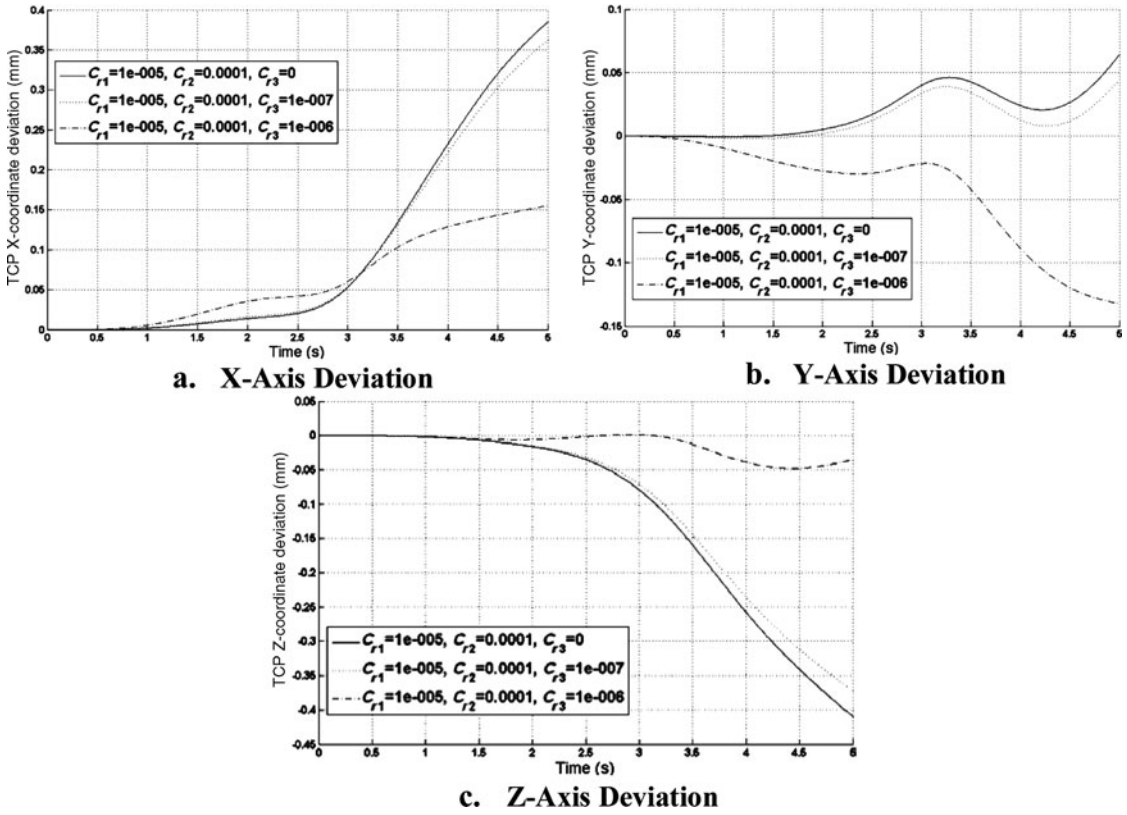

Fig. 23. Study of the overcrossing in coordinates with variable c_{r3}.

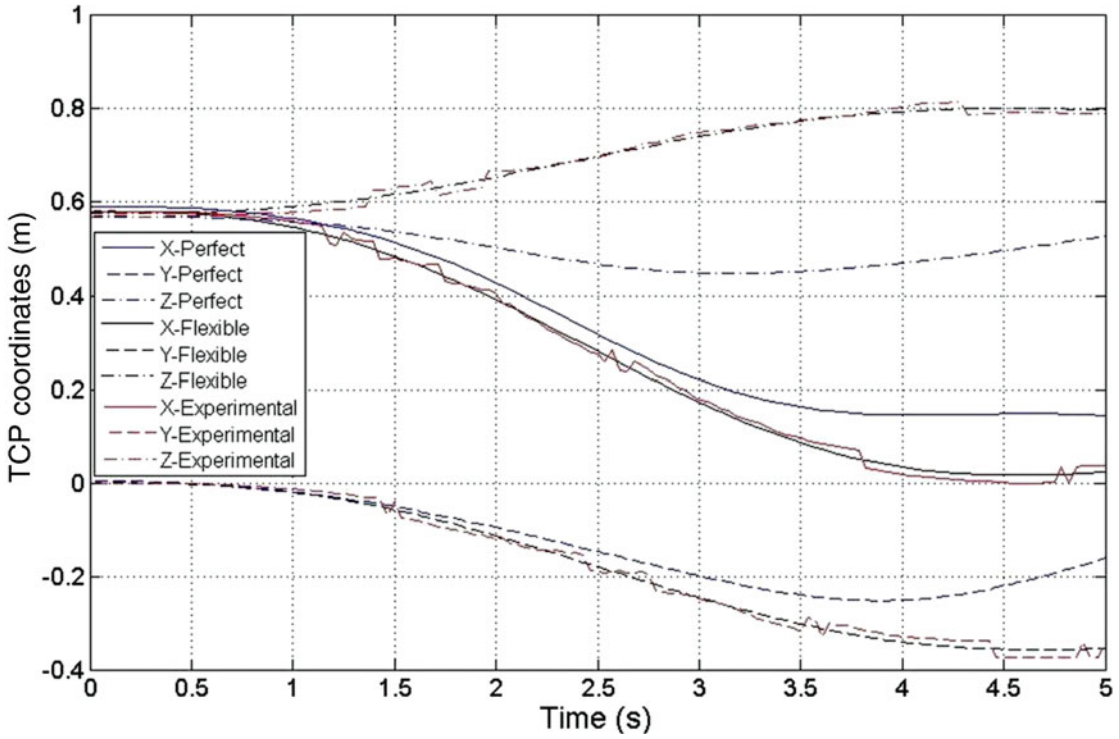

Fig. 24. TCP Cartesian coordinates.

https://doi.org/10.1017/S0263574714000848 Published online by Cambridge University Press

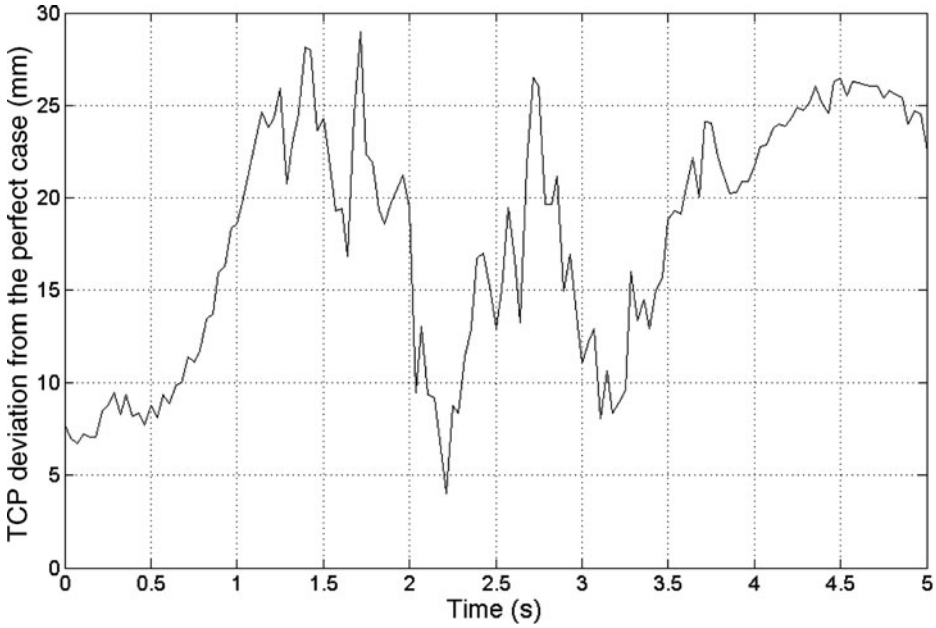

Fig. 25. Absolute TCP positional deviation.

experimental results give high deviation from that estimated via the simulation codes. However, the fluctuation of the absolute deviation (Fig. 25) suggests that low resolution cameras, and image processing mathematical errors contribution to the deviation is high. Also, the accumulative error of the physical system, poor quality rapidly deteriorating motors, as well as the contribution of the flexible joint itself contribute to the deviation.

6. Conclusions

This paper studies the effect of joints flexibilities on the dynamic performance of a serial robot arm of rigid links. Generalized dynamic models of n-link serial robot including a number of flexible joints is developed using multibody dynamics approach. A numerical algorithm and experimental test-rig are developed to simulate the obtained dynamic models in which Lagrange multipliers and numerical integration methods are implemented and applied to a three-link robot arm test-rig (SRLFJ) of type RRR. The approximate values of the joints' flexibility coefficients are estimated empirically. The obtained simulation results are compared with those of the ideal case of perfect geometry joints. The results show the significant contribution of joint damping to the robot inaccuracies A new model for flexible robot joints is developed. The experimental results agree to a large extent with the final developed model simulations. The experimental results show that the test-rig needs to be enhanced using more accurate equipment, and that the model neglects the unmodeled dynamics and errors in the parameter estimations. Further work to be done is to enhance upon the multibody model in order to improve on the flexibility model, improve the experimental setup to allow for more advanced control algorithms to be researched, and design a robust feedback controller for flexible joint robots.

References

1. M. W. Spong, "Modeling and control of elastic joint robots," *J. Dyn. Syst., Measure. Control* **109**(4), 310–319 (1987).
2. F. Ciuca, T. Lahdhiri and H. A. ElMaraghy, "Linear Robust Motion Control of Flexible Joint Robots Part A: Modeling," *Proceedings of the American Control Conference*, San Diego, CA, vol. 1 (Jun. 2–4, 1999) pp. 699–703.
3. V. Potkonjak, "Contribution to the dynamics and control of robots having elastic transmission," *Robotica* **6**, 63–69 (1988).
4. K. P. Jankowski and H. Van Brussel, "Inverse dynamics task control of flexible joint robots – Part I: Continuous time approach, Part II: Discrete-time approach," *Mech. Mach. Theory* **28**(6), 741–762 (1993).

https://doi.org/10.1017/S0263574714000848 Published online by Cambridge University Press

5. B. Subudhi and A. S. Morris, "Dynamic modeling, simulation and control of a manipulator with flexible links and joints," *Robot. Auton. Syst.* **41**, 257–270 (2002).
6. P. Flores, J. Ambrosio, J. C. P. Claro, H. M. Lankarani and C. S. Koshy, "A study on dynamics of mechanical systems including joint clearance and lubrication," *Mech. Mach. Theory* **41**, 247–261 (2006).
7. A. Heidari and A. Nikoobin, "Maximum Allowable Dynamic Load of Flexible Manipulators with Imposing Residual Vibration Constraint," *Proceedings of the IEEE International Conference on Robotics and Biomimetics*, Sanya (Dec. 15–18, 2007) pp. 1457–1462.
8. L. Le Tien, A. Albu-Schäffer, A. De Luca, G. Hirzinger, "Friction Observer and Compensation for Control of Robots with Joint Torque Measurement," *IEEE/RSJ International Conference on Intelligent Robots and Systems*, Nice (Sep. 22–26, 2008) pp. 3789–3795.
9. K. Melhem and A. Loria, "A New Model for Flexible Joint Robots," *IFAC, 15th Triennial World Congress*, 2002.
10. C. Ott, A. Albu-Schäffer, A. Kugi, and G. Hirzinger, "On the passivity-based impedance control of flexible joint robots," *IEEE Trans. Robot.* **24**(2), 416–429 (2008).
11. S. K. Ider and O. Korkmaz, "Trajectory tracking control of parallel robots in the presence of joint drive flexibility," *J. Sound Vibrat.* **319**, 77–90 (2009).
12. J. Dahai and L. Xiaoping, "On-line identification of time-varying physical parameters of robot joint based on harmonic propagation," *Chinese J. Mech. Eng.* **45**(3), 296–301 (2009).
13. W. Yang, J. Kwon, N.Y. Chong and Y. Oh, "Biologically inspired robotic arm control using an artificial neural oscillator," *Hindawi Publishing Corporation Mathematical Problems in Engineering* 2010, Article ID 107538, 16 pages. doi:10.1155/2010/107538.
14. S. E. Talole, J. P. Kolhe and S. B. Phadke, "Extended-extended-state-observer-based control of flexible-joint system with experimental validation," *IEEE Trans. Ind. Electron.* **57**(4), 1411–1419 (2010).
15. I. H. Akyuz, E. Yolacan, H. M. Ertunc and Z. Bingul, "PID and State Feedback Control of a Single-Link Flexible Joint Robot Manipulator," *Proceedings of IEEE International Conference on Mechatronics*, Istanbul, Turkey (Apr. 13–15, 2011) pp. 409–414.
16. G. Xue, X. Ren, K. Xing and Q. Chen, "Discrete-Time Sliding Mode Control Coupled with Asynchronous Sensor Fusion for Rigid-Link Flexible-Joint Manipulators," *IEEE International Conference on Control and Automation*, Hangzhou (Jun. 12–14, 2013) pp. 238–243.
17. A. A. Shabana, *Computational Dynamics* (John Wiley and Sons, New York, USA, 1994).
18. M. Zaher, Modeling and Simulation of Joints' Flexebility on the Dynamic Performance of Spatial Robots *M.Sc. Thesis* (Cairo University, Egypt, 2009).
19. A. A. Nada, B. A. Hussein, S. M. Megahed and A. A. Shabana, "Floating Frame of Reference and Absolute Nodal Coordinate Formulations in the Large Deformation Analysis of Robotic Manipulators: A Comparative Experimental and Numerical Study," *Proceedings of the ASME 2009 International Design Engineering Technical Conferences & Computers and Information in Engineering Conference IDETC/CIE 2009*, San Diego, USA (Aug. 30–Sep. 2, 2009).
20. A. A. Nada, *Flexible Robotic Manipulators: Modeling, Simulation and Control with Experimentation,* Doctoral Dissertation (Cairo University, Egypt, 2007).
21. A. J. Koivo, *Fundamentals for Control of Robotic Manipulators* (John Wiley and Sons, New York, USA, 1989).
22. S. M. Megahed, *Principles of Robot Modeling and Simulation* (John Wiley and Sons, New York, USA, 1993).
23. P. Eschmann, L. Hasbargen and K. Weigand, *Die Wälzlagerpraxis,* 2nd ed. (R. Oldenbourg Verlag, Munich, Germany, 1978).